

Theoretical and experimental assessment of structural, spectroscopic, electronic and nonlinear optical properties of two aroylhydrazone derivative

Füreyä Elif Öztürkkan Özbek^{a,*}, Güventürk Uğurlu^{b,*}, Erbay Kalay^c, Hacali Necefoğlu^{d,e}, Tuncer Hökelek^f

^a Department of Chemical Engineering, Kafkas University, 36100 Kars, Turkey

^b Department of Physics, Kafkas University, 36100 Kars, Turkey

^c Kars Vocational School, Kafkas University, 36100 Kars, Turkey

^d Department of Chemistry, Kafkas University, 36100 Kars, Turkey

^e International Scientific Research Centre, Baku State University, 1148 Baku, Azerbaijan

^f Department of Physics, Hacettepe University, 06800 Beytepe, Ankara, Turkey

ARTICLE INFO

Article history:

Received 8 June 2020

Revised 25 July 2020

Accepted 26 July 2020

Available online 30 July 2020

Keywords:

Aroylhydrazones

Single crystal XRD

Hirshfeld surface analysis

Spectroscopic characterization

Molecular electrostatic potential

Energy gap

ABSTRACT

Two aroylhydrazone, *N'*-(pyridine-4-ylmethylene)nicotic acid hydrazide (**1**) and *N'*-(pyridine-3-ylmethylene)nicotic acid hydrazide (**2**), were synthesized and their structures were determined by single-crystal X-ray diffraction analysis. The X-ray analysis indicated that the compound **1** was crystallized in triclinic crystal system with *P*-1 space group $a = 8.7899$ (2) Å, $b = 10.8983$ (3) Å, $c = 11.7726$ (3) Å, $\alpha = 89.952$ (3)°, $\beta = 88.684$ (3)°, $\gamma = 75.293$ (2)°, $V = 1090.50$ (5) Å³ and $Z = 4$ and compound **2** was crystallized in monoclinic crystal system with *P*2₁/*c* space group, $a = 11.9239$ (3) Å, $b = 8.6495$ (2) Å, $c = 11.1021$ (3) Å, $\alpha = 90$ (3)°, $\beta = 111.664$ (3) (3)°, $\gamma = 90$ °, $V = 1064.14$ (5) Å³ and $Z = 4$. Intermolecular interactions of the compounds were determined by Hirshfeld Surface Analysis. The H ... H interactions with 37.9% (for compound **1**) and 37.5% (for compound **2**) contributions are the most important interactions to the overall crystal packings. FT-IR, Raman, ¹H and ¹³C NMR and UV-Vis spectroscopy methods were used for spectroscopic characterization of the compounds. The spectroscopic properties of the compounds were calculated theoretically by using Density Functional Theory (DFT) with B3LYP and ab initio Hartree-Fock (HF) methods at different basis sets. A correlation was found between the theoretical and experimental values for the spectroscopic results. Moreover, the highest occupied molecular orbital (HOMO), the lowest unoccupied molecular orbital (LUMO), electric dipole moment (μ), polarizability (α) and hyperpolarizability (β) of the compounds were computed both DFT/B3LYP/6-311++G(d,p) and ab initio HF/6-311++G(d,p) methods. The calculated first hyperpolarizability value at the DFT/B3LYP/6-311++G (d,p) level of compound **1** with dimer structure is 18.14 times larger than urea, the standard nonlinear optical material. So, this value implies that compound **1** considered have potential candidates for designing high quality nonlinear optical materials. The energy gap (ΔE_{gap}) and Molecular Electrostatic Potential (MEP) of the compounds were investigated. The structural and vibration frequency values calculated theoretically were compared with the experimental values.

© 2020 Elsevier B.V. All rights reserved.

1. Introduction

In recent years, hydrazone ligands have increasingly attracted attention due to various features and extensive applications. Aroylhydrazones and their metal complexes are an excellent class of

compounds with biological prospects such as anticancer, antibacterial, antioxidant, and anti-HIV activities [1–4]. Interest in these ligands is due to the fact that the aromatic ring within them is a component of many biological systems. Aroylhydrazones have many interesting features structurally as well, with their degree of rigidity, the conjugated π system, and the protonated or deprotonated region in the NH group [5,6]. Aroylhydrazones which contain protonated or deprotonated potential donor atoms such as amido nitrogen and oxygen atoms and imino-nitrogen atoms

* Corresponding authors.

E-mail addresses: elif@kafkas.edu.tr (F.E. Öztürkkan Özbek), gugurlu@kafkas.edu.tr (G. Uğurlu).

are ideal ligands commonly used in coordination chemistry. These compounds containing the $-C(O)-NH-N=C-$ moiety are also identified as one of the versatile compounds that can make intermolecular hydrogen bonds. When evaluated in terms of functional groups, aroylhydrazones are unique ligands because they have a trinuclear azomethine group ($-C=N-NH-$) that provides structure diversity, a $C=N$ double bond that can form configuration isomerism, and $-C(=O)-HN-$ group that can form an intermolecular hydrogen bond ($C=O\cdots H-N$) that provides stability to the structure. Due to the physicochemical properties exhibited by the contribution of these structural characteristics, aroylhydrazone compounds are considered as interesting materials in industrial, pharmacological, and medicinal chemistry fields [7–11].

Computational chemistry is important in studying the properties of materials. Computational chemistry is fairly cheap, fast compared to an experiment, and environmentally safe. Even if it does not replace experiments, theoretical computation is so reliable in some ways that it is used today even before experimental processes are started [12]. Nowadays with the improvement of computer technology and the development of efficient computational methods, it is possible to perform detailed physicochemical measurements and quantum chemical calculations for organic molecules, at least in the gas phase, even on personal computers. By computer calculations, it is possible to calculate molecular properties such as energies and thermodynamic data, geometries, charge distributions, vibrations, magnetic resonance parameters, and reaction pathways [13]. Density functional theory (DFT) and ab initio Hartree-Fock (HF) are widely used methods in computational chemistry. In particular, the results obtained from DFT methods for molecular geometry, FT-IR, FT-Raman, UV-Vis, NMR spectra, etc. are highly compatible [14–16]. Although there are numerous studies on the synthesis, crystal structure and applications of aroylhydrazones and their metal complexes, studies on comparing experimental data with computerized methods are limited [17–24]. Synthesis, physical and antituberculosis properties of N' -(pyridin-4-ylmethylene)nicotic acid hydrazide (**1**) and N' -(pyridin-3-ylmethylene)nicotic acid hydrazide (**2**) were reported in a previous study by Kakimoto and Yamamoto [25]. In this study, two aroylhydrazones, N' -(pyridine-4-ylmethylene)nicotic acid hydrazide (**1**) and N' -(pyridine-3-ylmethylene)nicotic acid hydrazide (**2**), were synthesized through condensation of the corresponding aldehyde with nicotinic hydrazide, and their structures were determined by single-crystal X-ray diffraction method, and their spectroscopic properties were studied by FT-IR, FT-Raman, 1H NMR and ^{13}C NMR and UV-Vis spectroscopy. Intermolecular interactions of compounds were determined by the Hirshfeld surface analysis method. Also, the structure parameters, vibrational frequencies of FT-IR and Raman spectra of the compounds, 1H and ^{13}C NMR chemical shifts, HOMO, LUMO, ΔE_{gap} , MEP, μ , α and β values of the compounds have been computed by using DFT/B3LYP and HF with different basis sets.

2. Experimental

2.1. Chemicals and instruments

All chemicals and solvents were purchased commercially and used without further purification. Fourier-transform infrared (FT-IR) spectra and Raman spectra of the compounds were recorded in the range of $4000-400\text{ cm}^{-1}$ on an ALPHA-P Bruker FT-IR spectrometer with attenuated total reflection (ATR) detector and a WITec alpha 300 R Micro-Raman spectrometer from solid sample, respectively. UV-Vis spectra were obtained with a Perkin Elmer's LAMBDA 25 Spectrophotometer. 400 MHz 1H NMR spectra and 100 MHz ^{13}C NMR spectra were acquired on Bruker Nuclear Magnetic Resonance (NMR) Spectroscopy. Chemical shifts are reported

relative to tetramethylsilane (TMS) and dimethylsulfoxide (DMSO- d_6), which were used as internal standards. Chemical shifts (δ) are given in ppm, and coupling constants (J) are given in Hertz. The following abbreviations are used for multiplicities: s = singlet, d = doublet, t = triplet, q = quartet, dd = doublet of doublets and m = multiplet. Pyridine-3-carbohydrazone was prepared according to the literature [22].

2.2. General procedure for the synthesis of compounds (1 and 2)

General procedure for the synthesis of compounds **1** and **2** was given in Scheme 1. The pyridine-3-carbohydrazone (1.25 g, 9.12 mmol) was placed in a round necked-flask and dissolved in absolute ethanol (50 mL). To this mixture, the corresponding aromatic aldehyde (0.976 g, 9.12 mmol, 4-formyl pyridine for **1**, 3-formyl pyridine for **2**) and five drops of glacial acetic acid as the catalyst was added. The reaction mixture was stirred under reflux for 5 h. The desired compound was monitored by TLC analysis. After the reaction was complete, the reaction mixture was concentrated in vacuo. The residue was recrystallized from ethanol to give product.

N' -(pyridine-4-ylmethylene)nicotic acid hydrazide (1)

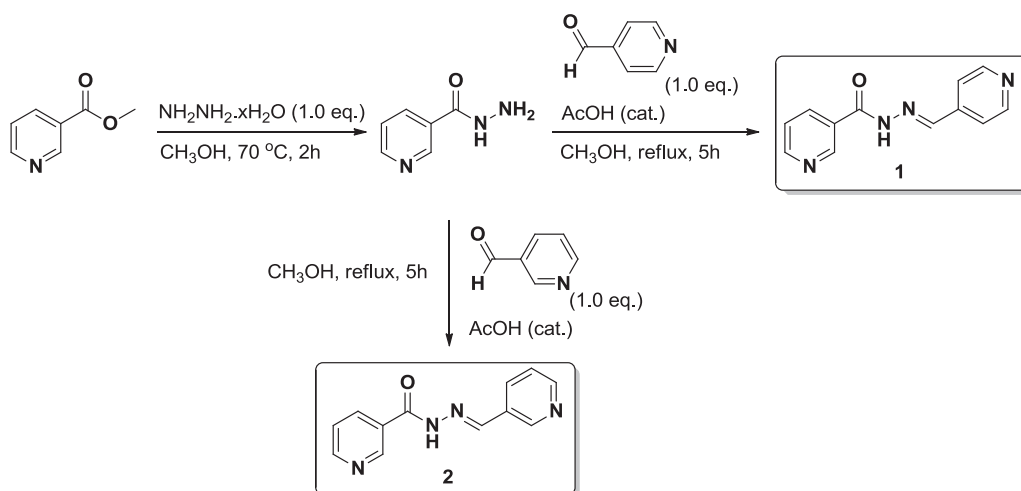
It was obtained as white solid, yield: 74%, m.p: 197–198 °C. IR (cm^{-1}) 3237, 3051, 3023, 2968, 2830, 1693, 1650, 1589, 1559, 1484, 1414, 1354 cm^{-1} . 1H NMR (400 MHz, DMSO- d_6 , ppm) δ 12.28 (s, 1H, NH), 9.11 (s, 1H, pyr CH), 8.77 (d, $J = 3.4$ Hz, 1H, pyr CH), 8.65–8.64 (m, 2H, pyr CH), 8.45 (s, 1H, N=CH), 8.28 (d, $J = 7.4$ Hz, 1H, pyr CH), 7.67 (d, $J = 3.9$ Hz, 2H, pyr CH), 7.56 (dd, $J = 7.4, 5.0$ Hz, 1H, pyr CH); ^{13}C NMR (100 MHz, DMSO- d_6 , ppm) δ 162.0 (Cq, C=O), 152.4 (CH), 150.2 (CH), 148.6 (CH), 145.9 (CH), 141.2 (Cq), 135.5 (CH), 128.8 (Cq), 123.5 (CH), 121.0 (CH) (Figs. S1 and S2).

N' -(pyridine-3-ylmethylene)nicotic acid hydrazide (2)

It was obtained as white solid, yield: 72%, m.p: 215–217 °C. IR (cm^{-1}) 3203, 3046, 2828, 1672, 1608, 1590, 1553, 1475, 1416, 1367, 1330 cm^{-1} . 1H NMR (400 MHz, DMSO- d_6 , ppm) δ 12.20 (s, 1H, NH), 9.06 (s, 1H, pyr CH), 8.87 (s, 1H, pyr CH), 8.76 (d, $J = 4.0$ Hz, 1H, pyr CH), 8.62 (d, $J = 4.0$ Hz, 1H, pyr CH), 8.49 (s, 1H, N=CH), 8.25 (d, $J = 7.8$ Hz, 1H, pyr CH), 8.15 (d, $J = 7.8$ Hz, 1H, pyr CH), 7.57 (dd, $J = 7.5, 4.9$ Hz, 1H, pyr CH), 7.49 (dd, $J = 7.5, 4.9$ Hz, 1H); ^{13}C NMR (100 MHz, DMSO- d_6 , ppm) δ 161.4 (Cq, C=O), 151.9 (CH), 150.4 (CH), 148.4 (CH), 148.2 (CH), 145.3 (CH), 135.0 (CH), 133.1 (CH), 129.6 (Cq), 128.6 (Cq), 123.6 (CH), 123.2 (CH) (Figs. S3 and S4).

2.3. X-ray crystallography

Single-crystal X-ray diffraction analyses of compounds **1** and **2** were performed on a Bruker SMART BREEZE CCD diffractometer using $Mo K_{\alpha}$ ($\lambda = 0.71073\text{ \AA}$) radiation at a temperature of 296 K [26]. Structures were solved by direct methods [27] and refined by full-matrix least squares against F^2 using all data [27]. All non-H atoms were refined anisotropically. Atoms H2A and H6A (for NH, in compound **1**) were located in difference Fourier maps and refined isotropically, while the N- and C-bound H atoms were positioned geometrically at distances of 0.86 Å (for NH, in compound **2**) and 0.93 Å (aromatic and methine CH) (in compounds **1** and **2**) from the parent C atoms; a riding model was used during the refinement processes and the $U_{iso}(H)$ values were constrained to be $1.2U_{eq}$ (carrier atom). Experimental data are given in Table 1.



Scheme 1. General procedure for the synthesis of compounds.

Table 1
Experimental details for compounds **1** and **2**.

Compounds	1	2
Empirical Formula	C ₁₂ H ₁₀ N ₄ O	C ₁₂ H ₁₀ N ₄ O
formula weight	226.24	226.24
color/shape	colourless/block	colourless/block
Crystal System	triclinic	monoclinic
Space Group	<i>P</i> $\bar{1}$	<i>P</i> 2 ₁ / <i>c</i>
<i>a</i> (Å)	8.7899 (2)	11.9239 (3)
<i>b</i> (Å)	10.8983 (3)	8.6495 (2)
<i>c</i> (Å)	11.7726 (3)	11.1021 (3)
α (°)	89.952 (3)	90
β (°)	88.684 (3)	111.664 (3)
γ (°)	75.293 (2)	90
<i>V</i> (Å ³)	1090.50 (5)	1064.14 (5)
<i>Z</i>	4	4
μ (Mo <i>K</i> α) (mm ⁻¹)	0.09	0.10
ρ (calcd) (mg m ⁻³)	1.378	1.412
Number of Reflections Total	47,702	6363
Number of Reflections Unique	5211	1948
<i>R</i> _{int}	0.048	0.077
2 θ _{max} (°)	56.80	53.20
<i>T</i> _{min} / <i>T</i> _{max}	0.688 / 0.744	0.618 / 0.745
Number of Parameters	315	155
GOF	1.24	1.27
<i>R</i> [<i>F</i> ² > 2 σ (<i>F</i> ²)]	0.086	0.117
w <i>R</i>	0.173	0.249
($\Delta\rho$) _{max} (e Å ⁻³)	0.25	0.28
($\Delta\rho$) _{min} (e Å ⁻³)	-0.28	-0.26

2.4. Computational details

Visualization and exploration of intermolecular close contacts of a structure is invaluable, and this can be achieved using the Hirshfeld surface (HS) [28–30]. HS analysis may be carried out to investigate the locations of atoms with potential to form hydrogen bonds and the quantitative ratios of these interactions. In the present study using Crystal Explorer 17.5 [31], To visualize the intermolecular interactions in the compounds **1** and **2**, the HS were mapped over *d*_{norm}, shape-index, curvedness and electrostatic potential. The electrostatic potential for compound **2** was calculated using TONTO [32,33] integrated into Crystal Explorer.

All the calculations were carried out with Gaussian 09, Revision B.01 [34] program package and supported by Gauss view 5.0 molecular visualization programs [35]. The initial molecular modeling of the compounds were optimized by using the density functional theory [36] treated according to hybrid Becke's three parameter and the Lee–Yang–Parr functional (B3LYP) [16,37,38] and ab-

Table 2
Hydrogen-bond geometry (Å, °).

Compound	D–H...A	D–H	H...A	D...A	D–H...A
1	N2–H2A...O2	0.86(3)	2.08(3)	2.866 (3)	151(3)
	N6–H6A...N1 ⁱ	0.94(3)	2.09(3)	3.003 (3)	165(3)
	C14–H14...N1 ⁱ	0.93	2.60	3.492 (4)	160
	C16–H16...N8 ⁱⁱ	0.93	2.61	3.497 (34)	159
2	N2–H2A...N4 ⁱⁱⁱ	0.86	2.32	3.124 (7)	155
	C2–H2...N4 ⁱⁱⁱ	0.93	2.56	3.474 (9)	166
	C3–H3...N1 ^{iv}	0.93	2.45	3.254(9)	145

Symmetry codes: (i) $-x + 2, -y, -z + 1$; (ii) $x + 1, y, z + 1$; (iii) $-x + 1, y - 1/2, -z + 1/2$; (iv) $x, -y + 1/2, z - 1/2$.

initio-Hartree-Fock (HF) [39] with 6–311+G for compound **1** and 6–311++G(d,p) basis sets [40,41] for compound **2** in the gas phase. After optimization, vibrational frequencies, HOMO, LUMO, μ , α and β values of the compounds were computed by using B3LYP/6–311++G (d,p) and HF/6–311++G (d,p) level of theory. By using the optimized parameters obtained theoretical calculations, The ¹H and ¹³C NMR chemical shifts were calculated with the GIAO method at the B3LYP/6–311+G (2d,p) and HF/6–311++G (d,p) level of theory. The MEP, LUMO and HOMO surfaces of compounds were plotted to visualize the charge distributions. The detailed vibrational assignments of theoretical FT-IR and Raman vibrational frequencies calculated with the DFT/B3LYP method were evaluated by means of vibrational energy distribution analysis (VEDA4) program [42].

3. Results and discussion

3.1. Single-crystal diffraction studies

The X-ray structural determinations of compounds **1** and **2** confirm the assignments of their structures from spectroscopic data. Selected experimental and theoretical bond lengths and angles are given in Supplemental Table 1. When the values obtained from single crystal X-ray diffraction method and DFT and HF calculations were compared, it was found that the values related to bond length and angles are compatible with each other. Hydrogen bond geometries are given in Table 2. The molecular structures along with the atom-numbering schemes are depicted in Fig. 1a and 1b, while the packing diagrams are given in Figs. S5a and S5b, respectively. In compound **1**, the asymmetric unit contains two crystallographically independent molecules, where they are linked by the intramolecular N–H...O hydrogen bond (Table 3 and Fig. 1a). The dihedral angles between the planar rings [A (N1/C1–C5) and

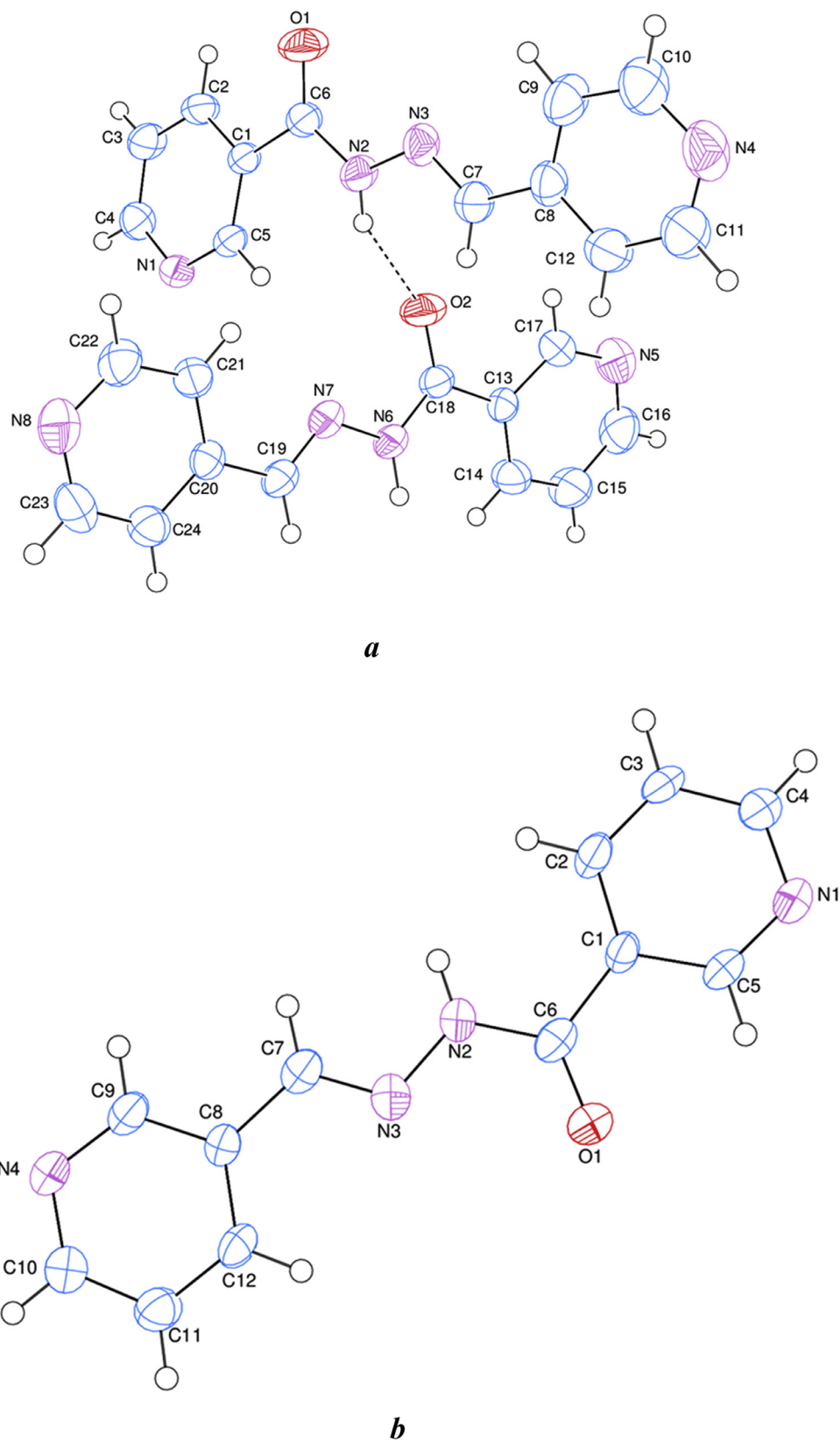


Fig. 1. **a.** An ORTEP-3 [50] view of compound 1. The thermal ellipsoids are drawn at the 50% probability level. N-H...O hydrogen bond is shown as dashed lines. **b.** An ORTEP-3 [50] view of compound 2. The thermal ellipsoids are drawn at the 50% probability level.

Table 3

Electronic Energy, dipole moment (μ), polarizability (α) hyperpolarizability (β), the highest occupied and lowest unoccupied molecular orbital Energies (E_{HOMO} and E_{LUMO}) of compound **1** and compound **2** (**1a** and **1b** are monomer units calculated for compound **1**).

DFT/B3LYP							
	Electronic Energy (a.u)	μ (D)	α (a.u)	β (a.u)	E_{HOMO} (a.u)	E_{LUMO} (a.u)	ΔE_{gap} (eV)
1	-1514.91984788	11.65	394.4	782.9	-0.237931	-0.108979	3.51
1a	-757.694635451	4.28	194.0	261.3	-0.257365	-0.092353	4.49
1b	-757.692978398	6.45	193.5	392.3	-0.258263	-0.092502	4.51
2	-757.693833408	4.13	194.5	236.9	-0.249646	-0.087209	4.42
HF							
1	-1505.41573923	12.67	338.9	311.0	-0.326544	0.011987	9.21
1a	-753.047377877	4.59	166.6	267.2	-0.348039	0.027391	10.22
1b	-753.045787879	6.81	166.5	311.0	-0.349282	0.021436	10.09
2	-753.047009248	4.44	167.1	52.4	-0.332221	0.024224	9.70

B (N4/C8–C12)] and $[C$ (N5/C13–C17) and D (N8/C20–C24)] are $A / B = 19.21(11)^\circ$ and $C / D = 7.09(9)^\circ$. In compound **2**, the asymmetric unit contains only one molecule, and the planar rings $[A$ (N1/C1–C5) and B (N4/C8–C12)] are oriented at a dihedral angle of $A / B = 4.26(18)^\circ$.

In the crystal structures of compounds **1** and **2**, there are intermolecular N–H ... N and C–H ... N hydrogen bonds (Table 2). In compound **1**, N–H ... O and N–H ... N hydrogen bonds (Table 2) link the molecules into centrosymmetric dimers (Fig. S5a), enclosing an $R_4^4(20)$ ring motif [43]. In compound **2**, N–H ... N hydrogen bonds (Table 2) link the molecules into infinite chains along the c -axis (Fig. S5b). The $\pi \cdots \pi$ interactions between the A , B , C and D rings, Cg1–Cg2ⁱ, Cg2–Cg2ⁱⁱ, Cg3–Cg3ⁱⁱⁱ and Cg3–Cg4^{iv} [symmetry codes: (i) $1 - x, 1 - y, 1 - z$; (ii) $1 - x, 1 - y, -z$; (iii) $2 - x, -y, 2 - z$; (iv) $2 - x, -y, 1 - z$, where Cg1, Cg2, Cg3 and Cg4 are the centroids of the rings A , B , C and D , respectively] (in compound **1**), and the $\pi \cdots \pi$ interactions between the A and B rings, Cg1–Cg2^v [symmetry code: (v) $1 - x, -y, -z$, where Cg1 and Cg2 are the centroids of the rings A and B , respectively] (in compound **2**) may stabilize the structures with the centroid-centroid distances of 3.957(2) Å, 3.671(2) Å, 3.808(2) Å and 3.816(2) Å (in compound **1**), and 3.779 (4) Å (in compound **2**).

The N1–C4, N1–C5, N2–N3, N2–C6 and N3–C7 bond lengths of compounds **1** and **2** were found to be 1.336 (3)/1.335 (8) Å, 1.341 (3)/1.341 (8) Å, 1.380 (3)/1.383 (7) Å, 1.355 (3) /1.354 (7) Å and 1.268 (3)/1.284 (7) Å and these bond lengths were calculated to be 1.3511/1.3377 Å, 1.3528/1.3325 Å, 1.375/1.3552 Å, 1.383/1.3897 Å and 1.2941/1.2798 Å in the B3LYP/6–311++g(d,p) and 1.3317/1.3211 Å, 1.3343/1.3163 Å, 1.3621/1.3545 Å, 1.3613/1.3708 Å and 1.2649/1.2517 Å in the HF/6–311++g(d,p) level of theory. In addition to, C4–N1–C5, N3–N2–C6 and N2–N3–C7 bond angles of compounds **1** and **2** were determined to be 117.3 (2)/116.2 (6)°, 120.6 (2)/119.0 (5) ° and 114.9 (2)/114.3 (5) ° and these angles were computed to be 118.48/117.59 °, 119.02/120.94 ° and 118.34/117.53 ° in the B3LYP/6–311++g(d,p) and 119.19/118.01 °, 119.09/119.90 ° and 119.52/117.93 ° in the HF/6–311++g(d,p) level of theory. The calculated bond lengths and bond angles are compatible with experimental values for both compounds.

3.2. Hirshfeld surface analysis

The d_{norm} (Figs. S6a and S6b), shape-index (Figs. S7a and S7b), curvedness maps (Fig. S8a and S8b) and electrostatic potential (only for compound **2**, Fig. S9) of compounds **1** and **2** were obtained with the help of Hirshfeld Surface Analysis. The electrostatic potential for compound **2** was mapped on the HS using STO-3 G basis set at Hartree-Fock level of theory over a range -0.1148 to 0.1274 au. The contact distances d_i and d_e from the HS to the near-

est atom inside and outside, respectively, enable the analysis of the intermolecular interactions through the mapping of d_{norm} . The combination of d_i and d_e in the form of two-dimensional fingerprint plots (Figs. 2 and 3) [44] provides a summary of intermolecular contacts in the crystal. In the HS with the d_{norm} (Fig. S6a and S6b) the white surface indicates contacts with distances equal to the sum of van der Waals radii, and the red and blue colours indicate distances shorter (in close contact) or longer (distant contact) than the Van der Waals radii, respectively [45]. The shape-index of the HS is a tool to visualize the $\pi \cdots \pi$ stacking by the presence of adjacent red and blue triangles (Figs. S7a and S7b) [46]. In the HS with curvedness (Figs. S8a and S8b) the curvature of the surface, with flat surfaces in green and curved regions in blue, is useful for depicting favourable stacking of the molecule in the crystal [47]. The electrostatic complementarity of the compound **2** is shown in Fig. S9. The blue regions indicate the positive electrostatic potential (hydrogen bond donors), while the red regions indicate the negative electrostatic potential (hydrogen bond acceptors) [33].

The overall two-dimensional fingerprint plots, Figs. 2a and 3a, (for compounds **1** and **2**, respectively) and those delineated into H ... H, H ... N / N ... H, H ... C / C ... H, C ... C, H ... O / O ... H, N ... C / C ... N, O ... C / C ... O, N ... N and O ... N / N ... O contacts (for compound **1**) and H ... H, H ... N / N ... H, H ... C / C ... H, H ... O / O ... H, C ... C, N ... C / C ... N, N ... N, O ... C / C ... O and O ... N / N ... O contacts (for compound **2**) [48] are illustrated in Fig. 2b–j and Fig. 3b–j, respectively, together with their relative contributions to the HS, where the significant H ... N / N ... H interactions are indicated by the pairs of wings in the two-dimensional fingerprint plots with the prominent long spikes at $d_e + d_i \approx 1.2$ Å (for compound **1**, Fig. 2c) and $d_e + d_i \approx 1.3$ Å (for compound **2**, Fig. 3c). According to the analysis results of the crystal structures, the most important interactions H ... H contributing 37.9% (for compound **1**) and 37.5% (for compound **2**) to the overall crystal packings, which are reflected in Figs. 2b and 3b as widely scattered points of high densities due to the large hydrogen contents of the molecules. The next important interactions are H ... N / N ... H, H ... C / C ... H, C ... C and H ... O / O ... H contributing 22.1%, 13.8%, 10.6% and 8.2% (for compound **1**), respectively, and H ... N / N ... H, H ... C / C ... H, H ... O / O ... H and C ... C contributing 19.6%, 13.6%, 12.1% and 8.6% (for compound **2**), respectively. The weakest intermolecular contacts contributing to the cohesions of the structures are N ... C / C ... N, O ... C / C ... O, N ... N and O ... N / N ... O, found to contribute only 4.4, 1.2, 1.1 and 0.7% (for compound **1**), respectively, and N ... C / C ... N, N ... N, O ... C / C ... O and O ... N / N ... O, found to contribute only 5.4, 1.7, 1.4 and 0.1% (for compound **2**), respectively (Fig. S10). The presence of these interactions may also be shown by the HS mapped as a function of curvedness (Figs. S8a and S8b). The large number of H ... H, H ... N / N ... H, H ... C / C ... H and H ... O / O ... H interactions suggest that Van der Waals inter-

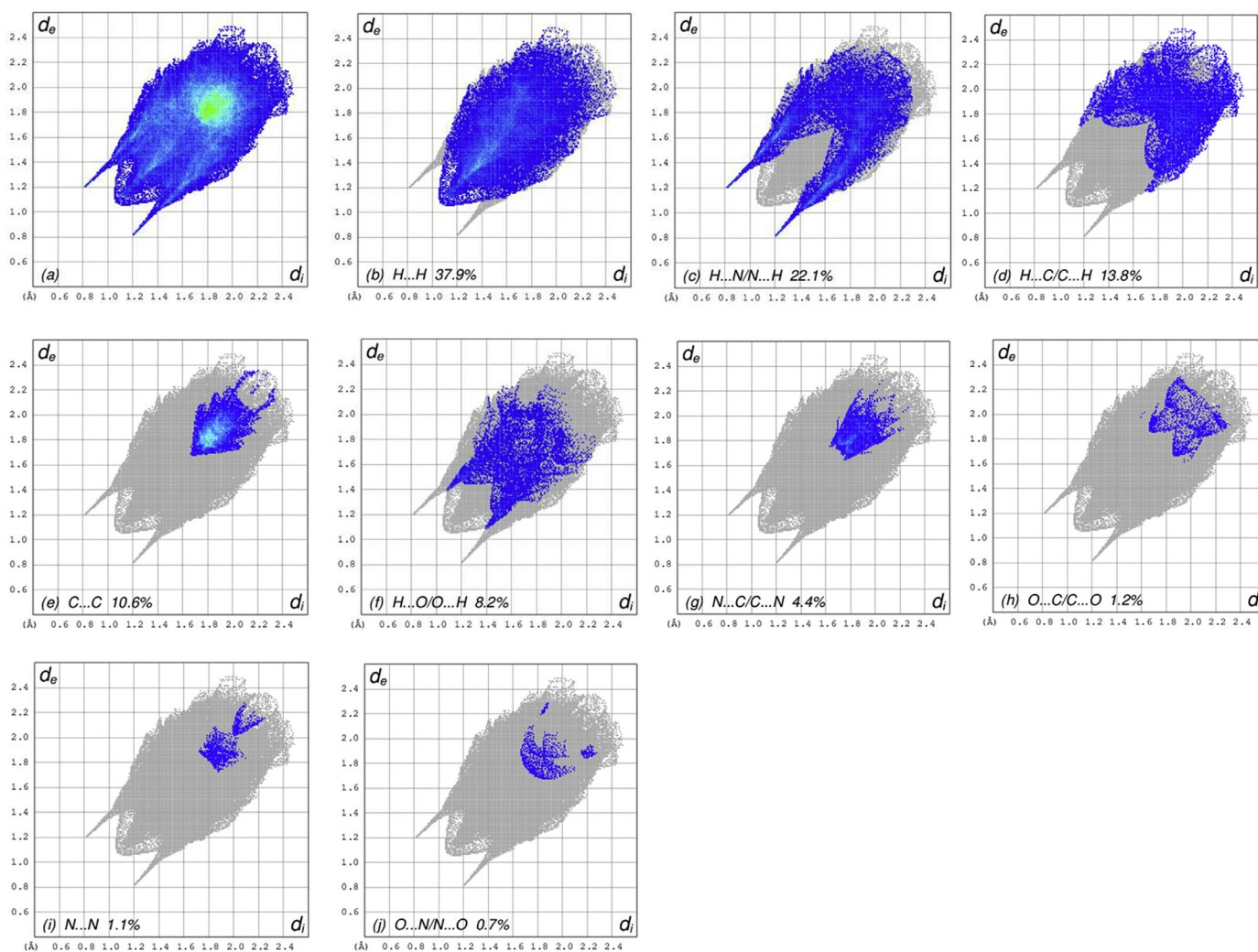


Fig. 2. The full two-dimensional fingerprint plots of compound **1** showing (a) all interactions and delineated into (b) H...H, (c) H...N/N...H, (d) H...C/C...H, (e) C...C, (f) H...O/O...H, (g) N...C/C...N, (h) O...C/C...O, (i) N...N and (j) O...N/N...O. The d_i and d_e are the closest internal and external distances (in Å) from given points on the Hirshfeld surface contacts.

actions and hydrogen bonding play the major roles in the crystal packings [49].

3.3. HOMO-LUMO and MEP analysis

The highest occupied molecular orbital and the lowest unoccupied molecular orbitals are important in terms of determine the electrical transport characteristic and calculate energies gap ($\Delta E_{\text{gap}} = E_{\text{LUMO}} - E_{\text{HOMO}}$) of the compounds. The energy levels of HOMO and LUMO were computed by the methods of B3LYP/6-311++G(d,p) of the compound **1** and compound **2** (Fig. 4). The theoretically calculated electronic energy, HOMO, LUMO, ΔE_{gap} , μ , α and β values monomer and dimer of the compound **1** and compound **2** obtained both methods were given in Table 3. As seen in Table 3, the dipole moment, polarizability and hyperpolarizability values of the dimer of the compound **1**, are larger than that of the monomer units, and the value of the energy gap (ΔE_{gap}) is smaller than that of the monomer units. The calculated ΔE_{gap} values of compound **1** and **2** are 3.51 and 4.42 eV at with DFT/B3LYP/6-311++G(d,p) level of theory and 9.21 and 9.70 eV at with HF/6-311++G(d,p) level of theory, respectively. As shown in Fig. 4, for both compounds, the HOMOs were localized over the entire molecules except for pyridine ring, whereas the LUMOs were mainly localized on the whole molecules.

Also, the β values of GAUSSIAN-09 output are given in atomic units (a.u.), the calculated hyperpolarizability value has been converted into electrostatic units (esu) (β : 1 a.u. = $0.0086393 \times 10^{-30}$ esu) [51]. The calculated β values of compound **1** and **2** are 6.764×10^{-30} and 2.047 esu, respectively. In the nonlinear optical study, urea is taken as the prototypical molecule and calculated β value at B3LYP/6-311++G(d,p) level of urea is $0.3728 \times 10^{-30} \text{ cm}^5 \text{ esu}^{-1}$ [52]. Thus, it was found that the calculated first hyperpolarizability values of compound **1** and **2** were 18.14 and 5.49 times greater than urea, the standard nonlinear optical material. According to this value obtained, compound **1** is a potential material for designing high quality nonlinear optical materials.

A molecular electrostatic potential is the interaction of a unit positive charge at a given point $p(x, y, z)$ in the surroundings of the molecule with the potential generated by the distribution of the electrical charge cloud density of the molecule. MEP provides important information about the electrostatic effect produced by the total charge distributions in the molecules, so it helps to understand molecular interactions. The MEP of the compound **1** and compound **2** obtained at the DFT/B3LYP/6-311G++ (d, p) level of theory were given in Fig. 5. As seen in Fig. 5, for compound **1**, the negative electrostatic potential (blue colored region) formed around O1, N2, N3, N4, and N8 atoms and positive potential (blue colored region) formed around the hydrogen atoms attached to N8

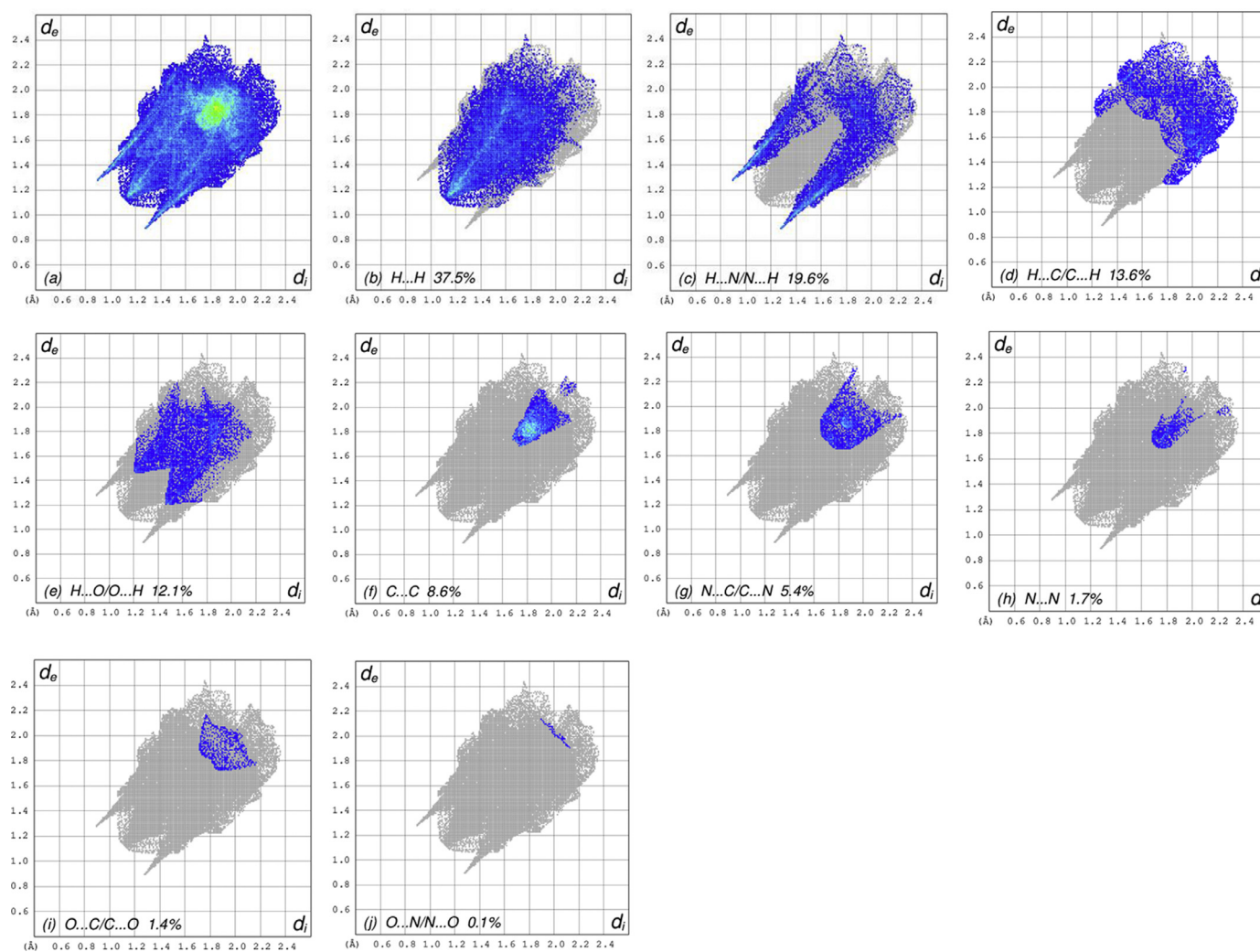


Fig. 3. The full two-dimensional fingerprint plot of compound **2**, showing (a) all interactions, and delineated into (b) H...H, (c) H...N/N...H, (d) H...C/C...H, (e) H...O/O...H, (f) C...C, (g) N...C/C...N, (h) N...N, (i) O...C/C...O and (j) O...N/N...O interactions. The d_i and d_e values are the closest internal and external distances (in Å) from given points on the Hirshfeld surface contacts.

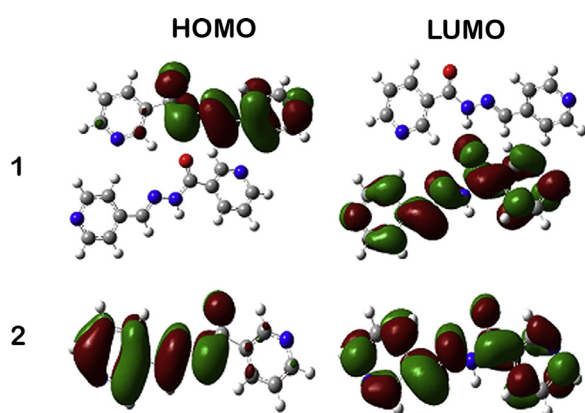


Fig. 4. 3D HOMO and LUMO plots on compound **1** and compound **2** (B3LYP/6-311++G(d,p)) results.

and C6 atom, for compound **2**, the negative electrostatic potential (blue colored region) formed around O1, N1 and N4 atoms and positive potential (red colored region) formed around the hydrogen atoms attached to N2 and C7 atoms.

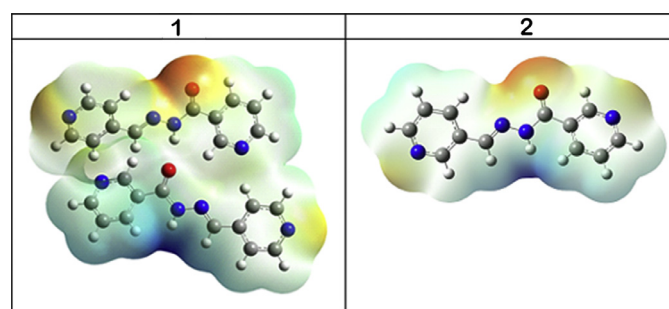


Fig. 5. 3D MEP plots on compound **1** and compound **2** according to the B3LYP/6-311++G(d,p) results.

3.4. Nuclear magnetic resonance spectra (NMR)

^1H and ^{13}C NMR spectra of the compounds **1** and **2** were recorded in DMSO- d_6 . The obtained these experimental data were compared with those obtained theoretically (Figs. S11 and S12). In the ^1H NMR spectra of the compounds **1** and **2**, the N-H proton observed as a singlet signal at 12.28 ppm and 12.20 ppm, respectively. A singlet signal belonged to N=C-H was showed at 8.45 ppm (for compound **1**) and 8.49 ppm (for compound **2**). The

aromatic protons of the pyridine rings of compounds **1** and **2** were observed among the 8.77–7.56 ppm and 8.77–7.47 ppm, respectively. When the chemical shift values of aromatic protons for Compound **1** were investigated in more detail, protons of H4 and H16 are experimentally found at 8.77 ppm as a doublet with value 3.4 Hz, while the H7 and H19 aromatic protons are observed as singlet resonance signal at 8.45 ppm. These protons were theoretically calculated at the interval of 8.22–9.48 ppm at B3LYP/6-311+g (2d,p) level and 8.63–8.97 ppm at HF/6-311++g(d,p) level, respectively. From the symmetry in the structure of compound **1**, H22, H23, H10 and H11 are identical protons. These protons give a resonance signal at 8.65 ppm. They were theoretically detected at the interval of 8.78–9.42 ppm at B3LYP/6-311+g (2d,p) level and 9.12–9.79 ppm at HF/6-311++g(d,p) level. The H9, H12, H21 and H24 which have the same chemical environment are observed as a doublet signal at 7.67 ppm with a value of 3.9 Hz within the most upfield aromatic proton region. The H3 proton was experimentally detected as doublets of doublet at 7.56 ppm with the value of coupling constants 5.0 Hz and 7.4 Hz splitting by the H2 and H4 protons and its calculated resonance signal is theoretically obtained at 9.12 ppm and 9.29 ppm at B3LYP/6-311+g (2d,p) and 9.91 ppm and 9.77 ppm HF/6-311++g(d,p) level, respectively. Similarly, when they aromatic proton resonances of compound **2** were also evaluated, the H5 and H9 protons resonance signals observed at 8.87 ppm and 9.06 ppm as a singlet, while they were theoretically calculated at 9.63 ppm and 8.81 ppm at B3LYP/6-311+g (2d,p) level and 9.84 ppm and 8.83 ppm at HF/6-311++g(d,p) level, respectively. The H4 and H10 protons are experimentally recorded as a doublet 8.76 ppm and 8.62 ppm with the coupling constant 4.0 Hz. The calculated values of these protons are found at 9.10 ppm and 8.94 ppm B3LYP/6-311+g (2d,p) level and 9.14 ppm and 8.99 ppm at HF/6-311++g(d,p) level respectively. H12 proton resonate as doublet at 8.25 ppm with a value of coupling constant 7.8 Hz splitting by H11 proton. In addition of this, H2 proton observed at 8.15 ppm as a doublet signal with a value of 7.8 Hz of coupling constant. The H11 proton, which interacted with the H10 and H12 protons, resonates as a doublets of doublet at 7.49 ppm. Finally, H3 aromatic proton was experimentally recorded as a doublets of doublet at 7.57 ppm with the value 4.9 Hz and 7.5 Hz of coupling constant. These protons were theoretically detected at 7.47 ppm at B3LYP/6-311+g (2d,p) level and 7.53 ppm at HF/6-311++g(d,p) level for the H11 proton and 7.37 ppm at B3LYP/6-311+g (2d,p) level and 7.36 ppm at HF/6-311++g(d,p) level for the H3. In ^{13}C NMR spectra, the C=O carbon signal for compound **1** and **2** was seen at 162 ppm and 161 ppm, respectively within downfield region of the ^{13}C NMR spectrum as expected. The aromatic carbon signals of compound **1** and **2** appeared at 152–123 ppm and 151–123 ppm, respectively [53–55]. The optimized molecular geometries of the compound **1** and **2** were determined by using DFT and HF methods with 6-31 G (d) basis level in DMSO solvent. Correlation graphs and linear correlation data obtained from ^1H and ^{13}C NMR experimental and theoretical spectra of Compounds **1** and **2** are given in Fig. S1-S4. The chemical shifts from ^1H NMR spectra obtained from experimental and B3LYP/6-31+G(d) and HF/6-31G+(d) methods were plotted. The chemical shifts from ^{13}C NMR spectra obtained from experimental and B3LYP/6-31G(d) and HF/6-31G(d) methods were plotted (Figs. S12). The R^2 values DFT/HF methods for ^1H NMR / ^{13}C NMR chemical shifts have been found as 0.7957/0.9733 and 0.5393/0.9288 for the compound **1**, respectively. Similarly, the R^2 values DFT/HF methods for ^1H NMR/ ^{13}C NMR chemical shifts have been found as 0.853/0.9672 and 0.6921/0.9309 for the compound **2**, respectively. There is a correlation between the experimentally and theoretically obtained chemical shifts except for N–H proton. O–H and N–H protons are known to be significantly affected by the solvent due to hydrogen bond and van der Waals interactions.

Chemical shifts in N–H protons in ^1H NMR of amine and amide compounds are a good example of their solvent action. However, this situation causes some deviations in the theoretical calculations. One of the best solvents used to eliminate this is DMSO. Although we used DMSO as solvent in our study, single crystal XRD and Hirshfeld surface analysis findings showed that the synthesized compounds have N–H ... O, C–H ... N and N–H ... N hydrogen bonds and Van der Waals interactions. Therefore, in the theoretical calculations, some chemical shifts were detected in the N–H protons [56–58]. It was determined that the data closest to the experimental data were those obtained with B3LYP/6-31+G(d) (for ^1H NMR) and B3LYP/6-31G(d) (for ^{13}C NMR) methods.

3.5. Vibrational analysis and UV studies

In the FT-IR spectra of the compound **1** and **2**, it was showed a medium vibration at 3237 cm^{-1} and 3203 cm^{-1} related to the $\nu(\text{N-H})$ stretching vibration, respectively. These absorption bands were computed at 3290 cm^{-1} (for DFT) and 3438 cm^{-1} (for HF) for **1** and 3345 cm^{-1} (DFT) and 3451 cm^{-1} (HF) for **2**. Both experimentally and theoretically, aromatic C–H vibrations were observed in the range of 3000–3050 cm^{-1} . The C=O and C=N vibrations were observed at 1693 cm^{-1} and 1650 cm^{-1} for **1** and 1672 cm^{-1} and 1608 cm^{-1} for **2**, respectively. These vibrations were calculated to be 1588 cm^{-1} and 1579 cm^{-1} for **1** and 1651 cm^{-1} and 1641 cm^{-1} for **2** with help of DFT and HF methods at 6–31 G, respectively. The $\nu(\text{N-N})$ stretching vibrations for **1** and **2** were observed at 1589 cm^{-1} and 1590 cm^{-1} , respectively. In FT-IR spectra obtained from DFT and HF calculations of compound **1** and **2**, the bands at 1530 cm^{-1} and 1584 cm^{-1} for **1** and 1574 cm^{-1} and 1604 cm^{-1} for **2** were assigned to $\nu(\text{N-N})$, respectively (Figs S13 and S14).

In the FT-Raman spectra of the compound **1** and **2**, the weak bands observed at 3250 cm^{-1} and 3240 cm^{-1} were assigned to N–H stretching vibrations, respectively. These vibrations were computed as 3645 cm^{-1} and 3656 cm^{-1} with help of DFT and HF methods for FT-Raman spectra, respectively. Similar to FT-IR spectra, aromatic C–H vibrations were also seen in the region of 3050–3000 cm^{-1} in FT-Raman spectra. The $\nu(\text{C=O})$, $\nu(\text{C=N})$ and $\nu(\text{N-N})$ vibrations were observed at 1604 cm^{-1} , 1589 cm^{-1} and 1544 cm^{-1} for **1**, respectively. The theoretically calculated values of these stretching vibrations were found to be 1604 cm^{-1} , 1574 cm^{-1} and 1499 cm^{-1} at DFT method and 1710 cm^{-1} , 1664 cm^{-1} and 1589 cm^{-1} at HF method. These vibrations for **2** were showed at 1629 cm^{-1} , 1589 cm^{-1} and 1550 cm^{-1} , respectively. The theoretically obtained values of these stretching vibrations were found to be 1682 cm^{-1} , 1603 cm^{-1} and 1537 cm^{-1} at DFT method and 1735 cm^{-1} , 1709 cm^{-1} and 1603 cm^{-1} at HF method. Characteristic C=O, C=C, and C=N vibrations were observed in 1688 cm^{-1} , 1602 cm^{-1} , and 1581 cm^{-1} , respectively, compared to similar reference acyl hydrazone compounds. In addition, all other observed vibrations were determined to be compatible with the literature [54,59–61]. The observed with respect to the starting compounds confirm that two new compounds are synthesized. In the infrared spectrum, it was observed that the C=N stretch of the related aldehyde and the N–H stretch bands of the acyl hydrazide was replaced by the new C=N stretch band in the product formed as a result of the condensation reaction of these two reagents. In addition, it was determined that the calculations obtained theoretically regarding the vibrations were compatible with the experimental data (Figs S15 and S16). The differences between the experimental and theoretical values of the above-mentioned vibrations can be attributed to non-covalent interactions such as intermolecular and intermolecular hydrogen bonds and Van der Waals interactions.

UV-Vis measurements of the compounds were recorded in DMSO. The $n \rightarrow \pi^*$ or $\pi \rightarrow \pi^*$ transitions resulting from the presence of pyridine ring, C=O, C=N were observed at 489 (**1**) and 386

(2) nm. The electronic energy excited states of compound 1 and 2 were calculated at TD-DFT/LSDA level with 6-31++G (d,p) and 6-311++G (d,p) in DMSO, respectively. The experimental and theoretical visible absorption maxima of the compound 1 and 2 are given in Fig. S17. These values at TD-DFT/LSDA/6-31++G (d,p) and TD-DFT/LSDA 6-311++G (d,p) level of theory were computed to be 452 and 393 nm, respectively. It was determined that the experimental and theoretical data of observed spectroscopic vibrations and electronic transitions are generally compatible.

4. Conclusions

In conclusion, *N'*-(pyridine-4-ylmethylene)nicotinic acid hydrazide (1) and *N'*-(pyridine-3-ylmethylene)nicotinic acid hydrazide (2) were synthesized. The spectroscopic properties, crystal structures of these compounds were investigated. The experimentally obtained data were compared with DFT with B3LYP and ab initio HF methods at different basis sets. Deviations in ¹H NMR and vibrational spectra theoretical calculations are attributed to non-covalent interactions such as intramolecular and intermolecular N-H ... O, C-H ... N and N-H ... N hydrogen bonds and Van der Waals interactions. The independent molecules for compound 1 connected each other via N-H ... O, C-H ... N and N-H ... N hydrogen bonds. N-H ... N hydrogen bonds provide stability to the crystal structure of compound 2. The π - π interactions between the pyridine rings also play an important role in the stability of the molecular architecture. H ... H, H ... N / N ... H, H ... C / C ... H, C ... C, H ... O / O ... H, N ... C / C ... N, O ... C / C ... O, N ... N and O ... N / N ... O interactions determined by Hirshfeld Surface analysis support the contribution of non-covalent and covalent interactions to the crystal structure. Also, DFT calculations at B3LYP/6-311++G(2d,p) and B3LYP/6-31G(d) levels are proposed as a suitable tool to estimate the crystal structure and spectroscopic properties of these compounds. In particular, compound 1 can be suggested as an ideal material for nonlinear optical applications with its calculated first hyperpolarizability value.

Declaration of Competing Interest

The authors declare that they have no known competing financial interests or personal relationships that could have appeared to influence the work reported in this paper.

Supplementary materials

Supplementary material associated with this article can be found, in the online version, at doi:10.1016/j.molstruc.2020.128982.

CRedit authorship contribution statement

Füreyä Elif Öztürkkan Özbek: Investigation, Writing - review & editing. **Güventürk Uğurlu:** Investigation, Writing - review & editing. **Erbay Kalay:** Investigation, Writing - review & editing. **Hacali Necefoğlu:** Investigation, Writing - review & editing. **Tuncer Hökelek:** Investigation, Writing - review & editing.

References

- [1] H.M.A. Abumelha, Synthesis and spectroscopic characterization of some hydrazone and 2 *H*-benzopyranone derivatives as antitumor agents: synthesis and spectroscopic characterization of some hydrazone and 2*H*-benzopyranone, *J. Heterocycl. Chem.* 55 (2018) 1738–1745, doi:10.1002/jhet.3211.
- [2] Y. Wu, X. Ding, L. Ding, Y. Zhang, L. Cui, L. Sun, W. Li, D. Wang, Y. Zhao, Synthesis and antibacterial activity evaluation of novel biaryloxazolidinone analogues containing a hydrazone moiety as promising antibacterial agents, *Eur. J. Med. Chem.* 158 (2018) 247–258, doi:10.1016/j.ejmech.2018.09.004.
- [3] U.P. Singh, H.R. Bhat, A. Verma, M.K. Kumawat, R. Kaur, S.K. Gupta, R.K. Singh, Phenyl hydrazone bearing pyrazole and pyrimidine scaffolds: design and discovery of a novel class of non-nucleoside reverse transcriptase inhibitors (NNRTIs) against HIV-1 and their antibacterial properties, *RSC Adv.* 3 (2013) 17335, doi:10.1039/c3ra41604f.
- [4] A. Budimir, T. Benković, V. Tomišić, A. Gojmerac Ivšić, N. Galić, Hydrolysis and extraction properties of aroylhydrazones derived from nicotinic acid hydrazide, *J. Solut. Chem.* 42 (2013) 1935–1948, doi:10.1007/s10953-013-0081-z.
- [5] P. Krishnamoorthy, P. Sathyadevi, R.R. Butorac, A.H. Cowley, N.S.P. Bhuvanesh, N. Dharmaraj, Variation in the biomolecular interactions of nickel(II) hydrazone complexes upon tuning the hydrazone fragment, *Dalton Trans.* 41 (2012) 6842, doi:10.1039/c2dt30121k.
- [6] Y. Li, Z. Yang, M. Zhou, Y. Li, J. He, X. Wang, Z. Lin, Ni(II) and Co(II) complexes of an asymmetrical aroylhydrazone: synthesis, molecular structures, DNA binding, protein interaction, radical scavenging and cytotoxic activity, *RSC Adv.* 7 (2017) 41527–41539, doi:10.1039/C7RA05504H.
- [7] H.K. Singh, R.K. Gupta, S.K. Singh, D.S.S. Rao, S.K. Prasad, A.S. Achalkumar, B. Singh, Synthesis and self-assembly of aroylhydrazone based polycatenars: a structure-property correlation, *J. Mol. Liq.* 284 (2019) 282–290, doi:10.1016/j.molliq.2019.04.003.
- [8] P.V. Bernhardt, J. Mattsson, D.R. Richardson, Complexes of cytotoxic chelators from the dipyrityl ketone isonicotinoyl hydrazone (HPKIH) analogues, *Inorg. Chem.* 45 (2006) 752–760, doi:10.1021/jc0515731.
- [9] H.H. Monfared, S. Sadighian, M.-A. Kamyabi, P. Mayer, Iron(III) aroylhydrazone complexes: structure, electrochemical studies and catalytic activity in oxidation of olefins, *J. Mol. Catal. A Chem.* 304 (2009) 139–146, doi:10.1016/j.molcata.2009.02.004.
- [10] B. Tang, H. Ma, G. Li, Y. Wang, G. Anwar, R. Shi, H. Li, Synthesis, crystal structures and luminescent properties of tetranuclear Zn molecular clusters with aroylhydrazone ligand, *CrystEngComm* 15 (2013) 8069, doi:10.1039/c3ce41034j.
- [11] D. Patra, N. Biswas, B. Kumari, P. Das, N. Sepay, S. Chatterjee, M.G.B. Drew, T. Ghosh, A family of mixed-ligand oxidovanadium(V) complexes with aroylhydrazone ligands: a combined experimental and computational study on the electronic effects of para substituents of hydrazone ligands on the electronic properties, DNA binding and nuclease activities, *RSC Adv.* 5 (2015) 92456–92472, doi:10.1039/C5RA17844D.
- [12] E.G. Lewars, *Computational Chemistry: Introduction to the Theory and Applications of Molecular and Quantum Mechanics*, 2. ed, Springer, Dordrecht, 2011.
- [13] B. Kirste, Applications of density functional theory to theoretical organic chemistry, *Chem. Sci. J.* 7 (2016), doi:10.4172/2150-3494.1000127.
- [14] M. Toy, H. Tanak, H. Şenöz, Experimental and DFT computational studies of novel 3-(*p*-cyanophenyl)-5-(*o,m,p*-nitrophenyl)-5-phenylformazans, *J. Mol. Struct.* 1213 (2020) 128178, doi:10.1016/j.molstruc.2020.128178.
- [15] F. De Proft, P. Geerlings, Conceptual and computational DFT in the study of aromaticity, *Chem. Rev.* 101 (2001) 1451–1464, doi:10.1021/cr9903205.
- [16] A.D. Becke, Density-functional thermochemistry. III. The role of exact exchange, *J. Chem. Phys.* 98 (1993) 5648–5652, doi:10.1063/1.464913.
- [17] J. Pisk, M. Rubčić, D. Kuzman, M. Cindrić, D. Agustin, V. Vrdoljak, Molybdenum(VI) complexes of hemilabile aroylhydrazone ligands as efficient catalysts for greener cyclooctene epoxidation: an experimental and theoretical approach, *New J. Chem.* 43 (2019) 5531–5542, doi:10.1039/C9NJ00229D.
- [18] M. Mohamadi, E. Faghieh-Mirzaei, S.Y. Ebrahimipour, I. Sheikhsaohaie, W. Haase, S. Foro, Synthesis, spectroscopic studies, DFT calculations, electrochemical evaluation, BSA binding and molecular docking of an aroylhydrazone-based cis-dioxido Mo(VI) complex, *J. Mol. Struct.* 1139 (2017) 418–429, doi:10.1016/j.molstruc.2017.03.047.
- [19] P. Rawat, R.N. Singh, Experimental and theoretical study of 4-formyl pyrrole derived aroylhydrazones, *J. Mol. Struct.* 1084 (2015) 326–339, doi:10.1016/j.molstruc.2014.12.045.
- [20] H. Hosseini-Monfared, R. Bikas, P. Mahboubi-Anarjan, A.J. Blake, V. Lippolis, N.B. Arslan, C. Kazak, Oxidovanadium(V) complexes containing hydrazone based O,N,O-donor ligands: synthesis, structure, catalytic properties and theoretical calculations, *Polyhedron* 69 (2014) 90–102, doi:10.1016/j.poly.2013.11.020.
- [21] N.A. Mathews, A. Jose, M.R.P. Kurup, Synthesis and characterization of a new aroylhydrazone ligand and its cobalt(III) complexes: X-ray crystallography and in vitro evaluation of antibacterial and antifungal activities, *J. Mol. Struct.* 1178 (2019) 544–553, doi:10.1016/j.molstruc.2018.10.061.
- [22] F. Elif Öztürkkan Özbek, G. Uğurlu, E. Kalay, H. Necefoğlu, Synthesis, characterization and computational studies of 4-[(Pyridine-3-carbonyl)-hydrazone(methyl)-benzoic acid, *J. Mol. Struct.* 1215 (2020) 128247, doi:10.1016/j.molstruc.2020.128247.
- [23] D. Dimić, The importance of specific solvent-solute interactions for studying UV-vis spectra of light-responsive molecular switches, *C. R. Chim.* 21 (2018) 1001–1010, doi:10.1016/j.crci.2018.09.007.
- [24] D. Dimić, M. Petković, Control of a photoswitching chelator by metal ions: DFT, NBO, and QTAIM analysis, *Int. J. Quantum Chem.* 116 (2016) 27–34, doi:10.1002/qua.25018.
- [25] S. Kakimoto, K. Yamamoto, Studies on antitubercular compounds. X. Condensation products of aldehydes and acid hydrazides of pyridine group, *Pharm. Bull.* 4 (1956) 4–6, doi:10.1248/cpb1953.4.4.
- [26] Bruker, APEX2, SAINT and SADABS, Bruker AXS Inc., Madison, Wisconsin, USA, 2012 n.d..
- [27] G.M. Sheldrick, A short history of SHELX, *Acta Crystallogr. Sect. A* 64 (2008) 112–122, doi:10.1107/S0108767307043930.

- [28] F.L. Hirshfeld, Bonded-atom fragments for describing molecular charge densities, *Theoret. Chim. Acta* 44 (1977) 129–138, doi:10.1007/BF00549096.
- [29] M.A. Spackman, J.J. McKinnon, Fingerprinting intermolecular interactions in molecular crystals, *CrystEngComm* 4 (2002) 378–392, doi:10.1039/B203191B.
- [30] M.A. Spackman, D. Jayatilaka, Hirshfeld surface analysis, *CrystEngComm* 11 (2009) 19–32, doi:10.1039/B818330A.
- [31] M.J. Turner, J.J. McKinnon, S.K. Wolff, D.J. Grimwood, P.R. Spackman, D. Jayatilaka, M.A. Spackman, *CrystalExplorer17*, University of Western Australia, 2017 n.d..
- [32] Jayatilaka, D., Grimwood, D.J., Lee, A., Lemay, A., Russel, A.J., Taylor, C., Wolff, S.K., Cassam-Chenai, P. & Whitton, A. (2005). TONTO. Available at: <http://hirshfeldsurface.net/>, (n.d.).
- [33] M.A. Spackman, J.J. McKinnon, D. Jayatilaka, Electrostatic potentials mapped on Hirshfeld surfaces provide direct insight into intermolecular interactions in crystals, *CrystEngComm* 10 (2008) 377–388, doi:10.1039/B715227B.
- [34] M. Frisch, G. Trucks, H. Schlegel, G. Scuseria, M. Robb, J. Cheeseman, G. Scalmani, V. Barone, B. Mennucci, G. Petersson, H. Nakatsuji, M. Caricato, X. Li, H. Hratchian, A. Izmaylov, J. Bloino, G. Zheng, J. Sonnenberg, M. Hada, M. Ehara, K. Toyota, R. Fukuda, J. Hasegawa, M. Ishida, T. Nakajima, Y. Honda, O. Kitao, H. Nakai, T. Vreven, J. Montgomery, J. Peralta, F. Ogliaro, M. Bearpark, J. Heyd, E. Brothers, K. Kudin, V. Staroverov, R. Kobayashi, J. Normand, K. Raghavachari, A. Rendell, J. Burant, S. Iyengar, J. Tomasi, M. Cossi, N. Rega, J. Millam, M. Klene, J. Knox, J. Cross, V. Bakken, C. Adamo, J. Jaramillo, R. Gomperts, R. Stratmann, O. Yazyev, A. Austin, R. Cammi, C. Pomelli, J. Ochterski, R. Martin, K. Morokuma, V. Zakrzewski, G. Voth, P. Salvador, J. Dannenberg, S. Dapprich, A. Daniels, Farkas, J. Foresman, J. Ortiz, J. Cioslowski, D. Fox, Gaussian 09, Revision B.01, Gaussian 09, Revision B.01, Gaussian, Inc., Wallingford CT. (2009).
- [35] Dennington R., Keith T., Millam J., Semichem Inc., GaussView, Version 5, Shawnee Mission KS, 2009. (n.d.).
- [36] W. Kohn, L.J. Sham, Self-consistent equations including exchange and correlation effects, *Phys. Rev.* 140 (1965) A1133–A1138, doi:10.1103/PhysRev.140.A1133.
- [37] C. Lee, W. Yang, R.G. Parr, Development of the Colle-Salvetti correlation-energy formula into a functional of the electron density, *Phys. Rev. B* 37 (1988) 785–789, doi:10.1103/PhysRevB.37.785.
- [38] B. Miehlich, A. Savin, H. Stoll, H. Preuss, Results obtained with the correlation energy density functionals of Becke and Lee, Yang and Parr, *Chem. Phys. Lett.* 157 (1989) 200–206, doi:10.1016/0009-2614(89)87234-3.
- [39] Chr. Møller, M.S. Plesset, Note on an approximation treatment for many-electron systems, *Phys. Rev.* 46 (1934) 618–622, doi:10.1103/PhysRev.46.618.
- [40] M.M. Francl, W.J. Pietro, W.J. Hehre, J.S. Binkley, M.S. Gordon, D.J. DeFrees, J.A. Pople, Self-consistent molecular orbital methods. XXIII. A polarization-type basis set for second-row elements, *J. Chem. Phys.* 77 (1982) 3654–3665, doi:10.1063/1.444267.
- [41] V.A. Rassolov, M.A. Ratner, J.A. Pople, P.C. Redfern, L.A. Curtiss, 6-31G* basis set for third-row atoms, *J. Comput. Chem.* 22 (2001) 976–984, doi:10.1002/jcc.1058.
- [42] M.H. Jamróz, Vibrational energy distribution analysis (VEDA): scopes and limitations, *Spectrochim. Acta Part A* 114 (2013) 220–230, doi:10.1016/j.saa.2013.05.096.
- [43] J. Bernstein, R.E. Davis, L. Shimon, N.-L. Chang, Patterns in hydrogen bonding: functionality and graph set analysis in crystals, *Angew. Chem. Int. Ed. Engl.* 34 (1995) 1555–1573, doi:10.1002/anie.199515551.
- [44] J.J. McKinnon, M.A. Spackman, A.S. Mitchell, Novel tools for visualizing and exploring intermolecular interactions in molecular crystals, *Acta Crystallogr., B* 60 (2004) 627–668, doi:10.1107/S0108768104020300.
- [45] P. Venkatesan, S. Thamotharan, A. Ilangoan, H. Liang, T. Sundius, Crystal structure, Hirshfeld surfaces and DFT computation of NLO active (2E)-2-(ethoxycarbonyl)-3-[(1-methoxy-1-oxo-3-phenylpropan-2-yl)amino] prop-2-enoic acid, *Spectrochim. Acta Part A* 153 (2016) 625–636, doi:10.1016/j.saa.2015.09.002.
- [46] S.K. Seth, G.C. Maity, T. Kar, Structural elucidation, Hirshfeld surface analysis and quantum mechanical study of para-nitro benzylidene methyl arjunolate, *J. Mol. Struct.* 1000 (2011) 120–126, doi:10.1016/j.molstruc.2011.06.003.
- [47] R. Soman, S. Sujatha, C. Arunkumar, Quantitative crystal structure analysis of fluorinated porphyrins, *J. Fluor. Chem.* 163 (2014) 16–22, doi:10.1016/j.jfluchem.2014.04.002.
- [48] J.J. McKinnon, D. Jayatilaka, M.A. Spackman, Towards quantitative analysis of intermolecular interactions with Hirshfeld surfaces, *Chem. Commun.* (2007) 3814–3816, doi:10.1039/b704980c.
- [49] V.R. Hathwar, M. Sist, M.R.V. Jørgensen, A.H. Mamakhel, X. Wang, C.M. Hoffmann, K. Sugimoto, J. Overgaard, B.B. Iversen, Quantitative analysis of intermolecular interactions in orthorhombic rubrene, *IUCr* 2 (2015) 563–574, doi:10.1107/S2052252515012130.
- [50] L.J. Farrugia, *WinGX and ORTEP for Windows*: an update, *J. Appl. Crystallogr.* 45 (2012) 849–854, doi:10.1107/S0021889812029111.
- [51] A.B. Ahmed, H. Feki, Y. Abid, H. Boughzala, A. Mlayah, Structural, vibrational and theoretical studies of L-histidine bromide, *J. Mol. Struct.* 888 (2008) 180–186, doi:10.1016/j.molstruc.2007.11.056.
- [52] J. Prashanth, G. Ramesh, J. Laxman Naik, J. Kishan Ojha, B. Venkatram Reddy, Molecular geometry, NBO analysis, Hyperpolarizability and HOMO-LUMO energies of 2-azido-1-phenylethanone using Quantum chemical calculations, *Mater. Today* 3 (2016) 3761–3769, doi:10.1016/j.matpr.2016.11.025.
- [53] R.M. Silverstein, F.X. Webster, D.J. Kiemle, D.L. Bryce (Eds.), *Spectrometric Identification of Organic Compounds*, Wiley, Hoboken, NJ, 2015.
- [54] R.K. Singh, A.K. Singh, S. Siddiqui, M. Arshad, A. Jafri, Synthesis, molecular structure, spectral analysis and cytotoxic activity of two new aroylhydrazones, *J. Mol. Struct.* 1135 (2017) 82–97, doi:10.1016/j.molstruc.2017.01.059.
- [55] N. Galić, A. Dijanošić, D. Kontrec, S. Miljanić, Structural investigation of aroylhydrazones in dimethylsulphoxide/water mixtures, *Spectrochim. Acta Part A* 95 (2012) 347–353, doi:10.1016/j.saa.2012.03.086.
- [56] H.C. Da Silva, W.B. De Almeida, Theoretical calculations of ¹H NMR chemical shifts for nitrogenated compounds in chloroform solution, *Chem. Phys.* 528 (2020) 110479, doi:10.1016/j.chemphys.2019.110479.
- [57] R.J. Abraham, J.J. Byrne, L. Griffiths, M. Perez, ¹H chemical shifts in NMR: Part 23, the effect of dimethyl sulphoxide versus chloroform solvent on ¹H chemical shifts, *Magn. Reson. Chem.* 44 (2006) 491–509, doi:10.1002/mrc.1747.
- [58] G.K. Pierens, T.K. Venkatachalam, D.C. Reutens, NMR and DFT investigations of structure of colchicine in various solvents including density functional theory calculations, *Sci. Rep.* 7 (2017) 5605, doi:10.1038/s41598-017-06005-5.
- [59] B.H. Stuart, *Infrared Spectroscopy: Fundamentals and Applications*, Wiley, Chichester, 2008.
- [60] P.J. Larkin, *Infrared and Raman Spectroscopy: Principles and Spectral Interpretation*, Elsevier, Amsterdam, 2011.
- [61] Ł. Popiołek, A. Biernasiuk, A. Malm, Synthesis and antimicrobial activity of new 1,3-thiazolidin-4-one derivatives obtained from carboxylic acid hydrazides, *Phosphorus Sulfur Silicon Relat. Elem.* 190 (2015) 251–260, doi:10.1080/10426507.2014.919293.